Current Biology 20, 1840–1845, October 26, 2010 ©2010 Elsevier Ltd All rights reserved DOI 10.1016/j.cub.2010.09.012

Report

# Cse1l Is a Negative Regulator of CFTR-Dependent Fluid Secretion

Michel Bagnat,[1,2,*] Adam Navis,[1] Sara Herbstreith,[1] Koroboshka Brand-Arzamendi,[2] Silvia Curado,[2] Sherif Gabriel,[3] Keith Mostov,[4] Jan Huisken,[2] and Didier Y.R. Stainier[2,*]

[1]Department of Cell Biology, Duke University School of Medicine, Durham, NC 27710, USA
[2]Department of Biochemistry & Biophysics, University of California, San Francisco, San Francisco, CA 94158-2324, USA
[3]Cystic Fibrosis and Pulmonary Diseases Research and Treatment Center, The University of North Carolina at Chapel Hill, NC 27599, USA
[4]Department of Anatomy, University of California, San Francisco, San Francisco, CA 94143-2140, USA

## Summary

**Transport of chloride through the cystic fibrosis transmembrane conductance regulator (CFTR) channel is a key step in regulating fluid secretion in vertebrates [1, 2]. Loss of CFTR function leads to cystic fibrosis [1, 3, 4], a disease that affects the lungs, pancreas, liver, intestine, and vas deferens. Conversely, uncontrolled activation of the channel leads to increased fluid secretion and plays a major role in several diseases and conditions including cholera [5, 6] and other secretory diarrheas [7] as well as polycystic kidney disease [8–10]. Understanding how CFTR activity is regulated in vivo has been limited by the lack of a genetic model. Here, we used a forward genetic approach in zebrafish to uncover CFTR regulators. We report the identification, isolation, and characterization of a mutation in the zebrafish *cse1l* gene that leads to the sudden and dramatic expansion of the gut tube. We show that this phenotype results from a rapid accumulation of fluid due to the uncontrolled activation of the CFTR channel. Analyses in zebrafish larvae and mammalian cells indicate that Cse1l is a negative regulator of CFTR-dependent fluid secretion. This work demonstrates the importance of fluid homeostasis in development and establishes the zebrafish as a much-needed model system to study CFTR regulation in vivo.**

## Results and Discussion

Following a genetic screen designed to identify mutants with defects in gut, liver, or pancreas organogenesis [11], we identified a recessive mutation, *s866* (22.4% penetrance, n = 548), which causes a striking gut phenotype. In *s866* mutants, internal organs appear to develop normally until 96–100 hr postfertilization (hpf), at which time the gut tube undergoes a process of expansion that results in a dramatically enlarged, fluid-filled tube (Figure 1). We named this mutant *baobab* (*bao*), after the African tree that accumulates water in its trunk. Using confocal microscopy, we observed that *bao*$^{s866}$ mutants develop a flat epithelium (devoid of folds) lining the lumen of this enlarged intestinal tube (Figures 1A–1E). Occasionally, delaminating cells were observed. However, *bao*$^{s866}$ mutants still exhibit gut peristalsis, and the intestinal cells retain apical membrane polarity, cadherin localization, tight junctions, and basal laminin deposition (data not shown). Using transmission electron microscopy, we observed a dramatic reduction in cell height and microvilli length in *bao*$^{s866}$ mutant enterocytes (Figures 1D and 1E). Nevertheless, *bao*$^{s866}$ mutant enterocytes retain expression and localization of the absorptive cell marker 4e8 [12] (see Figure S1A available online). Although all delaminating cells in *bao*$^{s866}$ mutants appeared to undergo apoptosis, we did not observe a significant increase in apoptosis in mutants compared to wild-type (WT) (Figure S1B). *bao*$^{s866}$ mutants also exhibit exocrine pancreas degeneration and liver growth arrest after 96 hpf (Figure S1C).

To define the events leading to gut lumen expansion in *bao*$^{s866}$ mutants, we first imaged the process from 96 to 120 hpf in larvae expressing histone 2A:GFP [13] using selective plane illumination microscopy [14]. This approach allowed us to visualize the shape and size of the gut tube and follow cell divisions. In WT larvae, the gut showed only a relatively small (46%) and steady increase in tube diameter between 96 and 120 hpf (Figure 1H). Gut tube growth in WT was mostly due to cell divisions, increased folding of the epithelium, and an increase in cell height associated with enterocyte polarization (see also Figures 1B and 1C) but not to changes in luminal volume. In contrast, lumen expansion in the mutant was dramatic (511%) and rapid, taking place in approximately 200 min, and without cell division (Figures 1F and 1G).

Next, we investigated the causes of gut lumen expansion in *bao*$^{s866}$ mutants. At the tissue level, this phenotype is reminiscent of what occurs in the gut of mice exposed to cholera toxin [5], where the lumen is greatly enlarged by the CFTR-dependent accumulation of fluid [9]. *CFTR* (cystic fibrosis transmembrane conductance regulator) is a vertebrate-specific gene [1]. Zebrafish Cftr shows 55% identity and 75% similarity to human CFTR and is highly expressed in the gut by 4 days postfertilization (see below and A.N. and M.B., unpublished data). To test whether lumen expansion in *bao*$^{s866}$ mutants is CFTR dependent, we treated WT and mutant larvae with CFTR inhibitors from 72 to 120 hpf. Various CFTR inhibitors (glibenclamide, CFTR172, and T08) effectively reduced the appearance of severely enlarged guts in *bao*$^{s866}$ mutants (84% reduction for 5 μM T08, a CFTR172 analog [10]; n = 1017 in total, 242 mutants) (Figure 2A). In addition, treatment of *bao*$^{s866}$ mutants with the CFTR inhibitor T08 significantly increased enterocyte height and microvilli length to levels close to WT (Figure S4). Although the CFTR inhibitors blocked lumen expansion, they did not prevent cell delamination, suggesting that cell delamination/apoptosis and lumen expansion are two separable phenotypes.

We next investigated the effects of CFTR activation. Soaking 120 hpf WT larvae in water containing a specific CFTR activator [15] (15 μM CFTR-Act9) led to a robust and reversible accumulation of fluid, resulting in a dramatic expansion of the gut lumen and the flattening of enterocytes in half of the larvae (50.8%, n = 360) (Figure 2Ba; Figure S2). This response had kinetics and appearance (i.e., reduction in cell height and

*Correspondence: m.bagnat@cellbio.duke.edu (M.B.), didier.stainier@ucsf.edu (D.Y.R.S.)

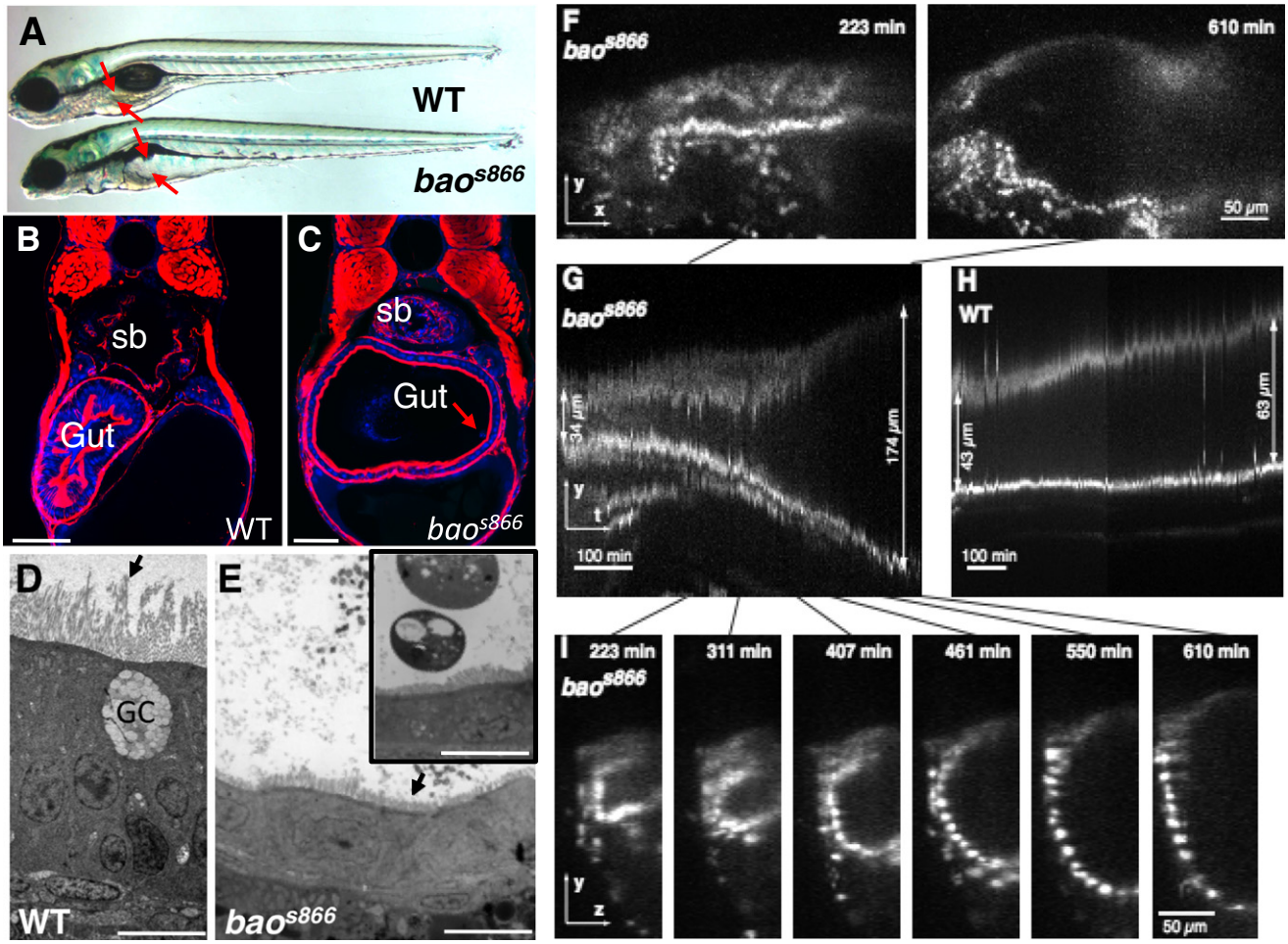


Figure 1. *bao*$^{s866}$ Mutants Undergo a Dramatic and Rapid Expansion of the Gut Lumen between 96 and 120 Hours Postfertilization

(A) Bright-field image of 120 hr postfertilization (hpf) wild-type (WT) and *bao*$^{s866}$ mutant larvae. Arrows point to the edges of the gut lumen.

(B and C) Confocal images of cross-sections of 120 hpf WT (B) and *bao*$^{s866}$ mutant (C) larvae. The arrow in (C) points to a delaminating cell. Red is F-actin and blue is DAPI; sb indicates swim bladder. Scale bars represent 50 μm.

(D and E) Dramatic shortening of microvilli (arrows) in *bao*$^{s866}$ mutant enterocytes observed by transmission electron microscopy at 120 hpf. Inset in (E) shows remnants of apoptotic cells found in the lumen. GC indicates goblet cell. Scale bars represent 10 μm.

(F–I) Rapid expansion of the gut lumen in *bao*$^{s866}$ mutants expressing histone 2A:GFP.

(F) Still images (lateral views) from a *bao*$^{s866}$ mutant selective plane illumination microscopy (SPIM) recording between 96 and 120 hpf showing first and last frames.

(G and H) Kymographs from *bao*$^{s866}$ mutant (G) and WT (H) gut. Lumen expansion in the mutant occurred in ~200 min; no cell division was observed.

(I) Still images (lateral views) from the *bao*$^{s866}$ mutant SPIM recording corresponding to the kymograph shown in (G).

microvilli length) similar to those observed upon lumen expansion in *bao*$^{s866}$ mutants but did not cause cell delamination (Figure 2Bb; Figure S4). Altogether, our data indicate that the increase in lumen size observed in *bao*$^{s866}$ mutants results from the uncontrolled, CFTR-dependent accumulation of fluid in the gut lumen. Because the *bao*$^{s866}$ mutation is recessive, it follows that Bao is a negative regulator of CFTR-dependent fluid secretion.

Because CFTR is regulated at multiple levels, including transcriptional and posttranscriptional stages, it is possible that the increased CFTR activity observed in *bao*$^{s866}$ mutants is due to increased expression and/or differences in subcellular localization of the channel. To investigate these possibilities, we raised an antibody against zebrafish Cftr. In western blots, the antibody recognized a protein of approximately 190 kDa (Figure S3A). Importantly, the signal was dramatically reduced in extracts prepared from larvae injected with an antisense morpholino against Cftr compared to uninjected controls (Figure S3A), indicating that the antibody recognizes CFTR specifically. In transverse sections, the antibody stained the apical surface of gut epithelial cells (Figure S3B). Western blot and immunohistological analyses revealed that Cftr protein levels and localization were not significantly different in *bao*$^{s866}$ mutants compared to WT (Figure 2C). These data suggest that Bao regulates CFTR-dependent fluid secretion by controlling CFTR activity and rule out transcriptional regulation, changes in CFTR steady-state levels, or subcellular distribution. However, we cannot exclude the possibility that differences in CFTR recycling [16], which would be very difficult to discern in vivo, also contribute to the increase in CFTR activity observed in *bao*$^{s866}$ mutants.

To gain molecular insight into the cellular processes controlled by the Bao protein, we undertook a positional cloning project to isolate the corresponding gene. Using

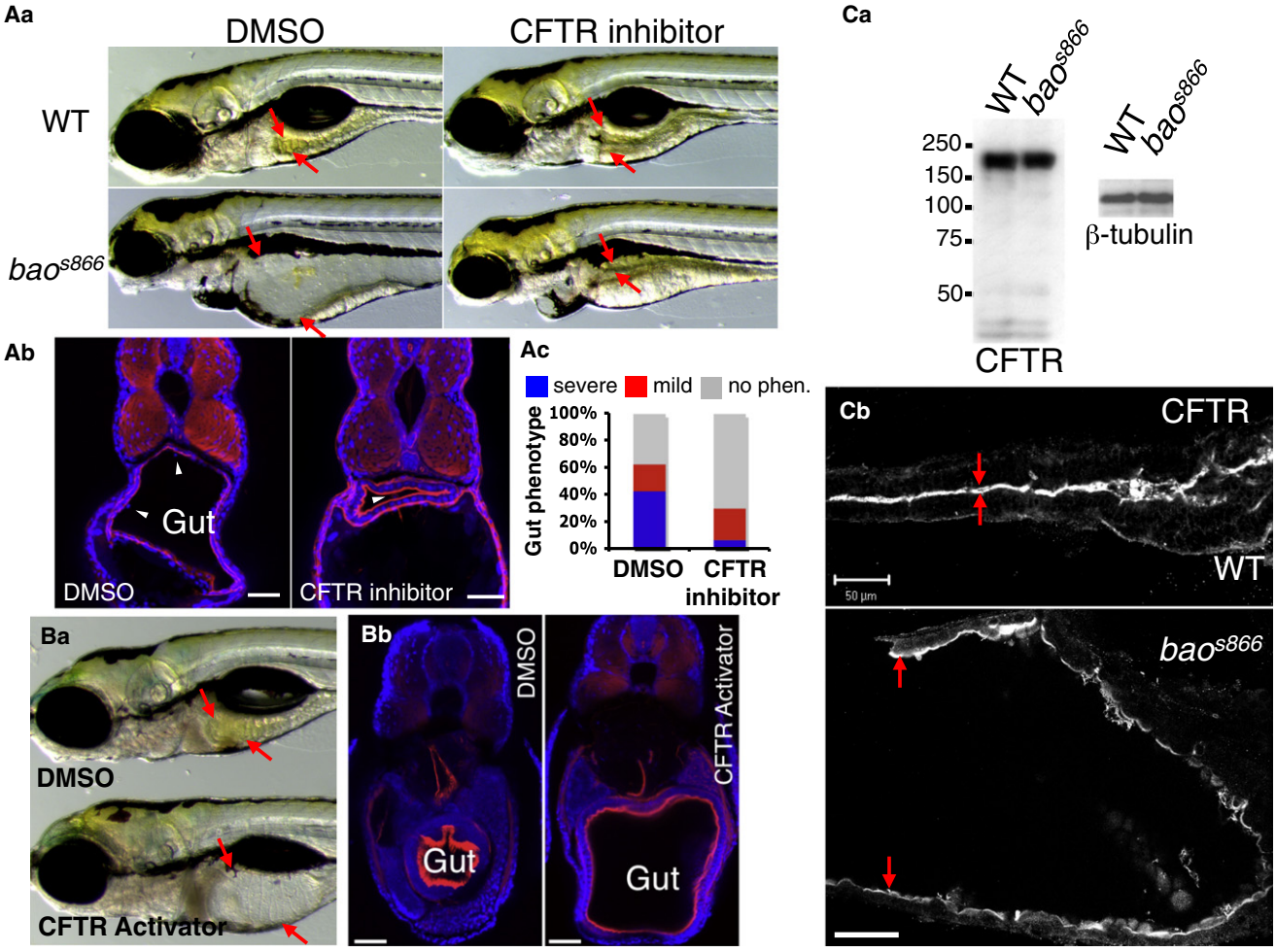


Figure 2. Lumen Expansion in *bao*$^{s866}$ Mutants Results from Increased CFTR-Dependent Fluid Secretion

(A) Inhibition of CFTR blocks lumen expansion in *bao*$^{s866}$ mutants.

(Aa) Bright-field images of WT and *bao*$^{s866}$ mutants incubated with DMSO (0.1%) or the CFTR inhibitor T08 (5 μM) from 72 to 120 hpf. Arrows point to the edges of the gut lumen.

(Ab) Confocal images of cross-sections of 144 hpf control and T08-treated *bao*$^{s866}$ mutants. Arrowheads point to delaminating cells. Red is F-actin and blue is DAPI. Scale bars represent 50 μm.

(Ac) Quantification of the gut phenotype in control and T08-treated *bao*$^{s866}$ mutants. Larvae were placed in three phenotypic categories (no phenotype, mild phenotype, or severe phenotype) and then genotyped.

(B) Activation of CFTR in WT phenocopies the gut lumen expansion defect of *bao*$^{s866}$ mutants.

(Ba) Bright-field image of 144 hpf WT larvae treated with DMSO (0.15%) or CFTR-Act9 (15 μM). Arrows point to the edges of the gut lumen.

(Bb) Confocal images of cross-sections of 144 hpf control and CFTR-Act9-treated WT larvae. Red is F-actin and blue is DAPI. Scale bars represent 20 μm.

(C) Cftr expression and localization is not affected in *bao*$^{s866}$ mutants compared to WT.

(Ca) Immunoblot of 120 hpf WT and *bao*$^{s866}$ mutants probed against Cftr and β-tubulin.

(Cb) Confocal images of whole mounts of 120 hpf WT (top) and *bao*$^{s866}$ mutant (bottom) stained for Cftr. Arrows point to the apical surface of the gut. Anterior is to the right. Scale bars represent 50 μm.

standard genetic mapping techniques, we defined a critical genomic interval on chromosome 12 containing only two genes, *chromosome segregation 1-like* (*cse1l*) and *protein tyrosine phosphatase receptor gamma* (*ptprg*) (Figure 3A). Next, we isolated cDNAs from WT and mutant larvae for both genes. Sequencing of these cDNAs revealed the absence of exon 16 in the middle of the *cse1l* transcript leading to a predicted premature stop codon in the next exon (Figures 3B and 3C). No mutations were found in the *ptprg* cDNA. Genomic DNA sequencing revealed a T-to-A mutation upstream of the exon 16 splice acceptor site (Figure 3B). We confirmed the aberrant splicing of exon 16 in the mutant by reverse transcriptase PCR on pools of RNA made from *bao*$^{s866}$ mutants and WT siblings (Figure 3C). Cse1l was depleted in extracts prepared from *bao*$^{s866}$ mutants compared to WT siblings as judged by immunoblots using antibodies against the N terminus of human CSE1L (Figure 3Da). However, we could not unequivocally detect the predicted truncated form of the protein in extracts made from *bao*$^{s866}$ mutants as a result of the presence of a cross-reacting protein of the same size (asterisk in Figure 3Da). To determine whether the mutant cDNA produces a truncated protein, we transfected HEK293 cells and performed an immunoblot analysis. The mutant cDNA produced a polypeptide of approximately 60 kDa, in

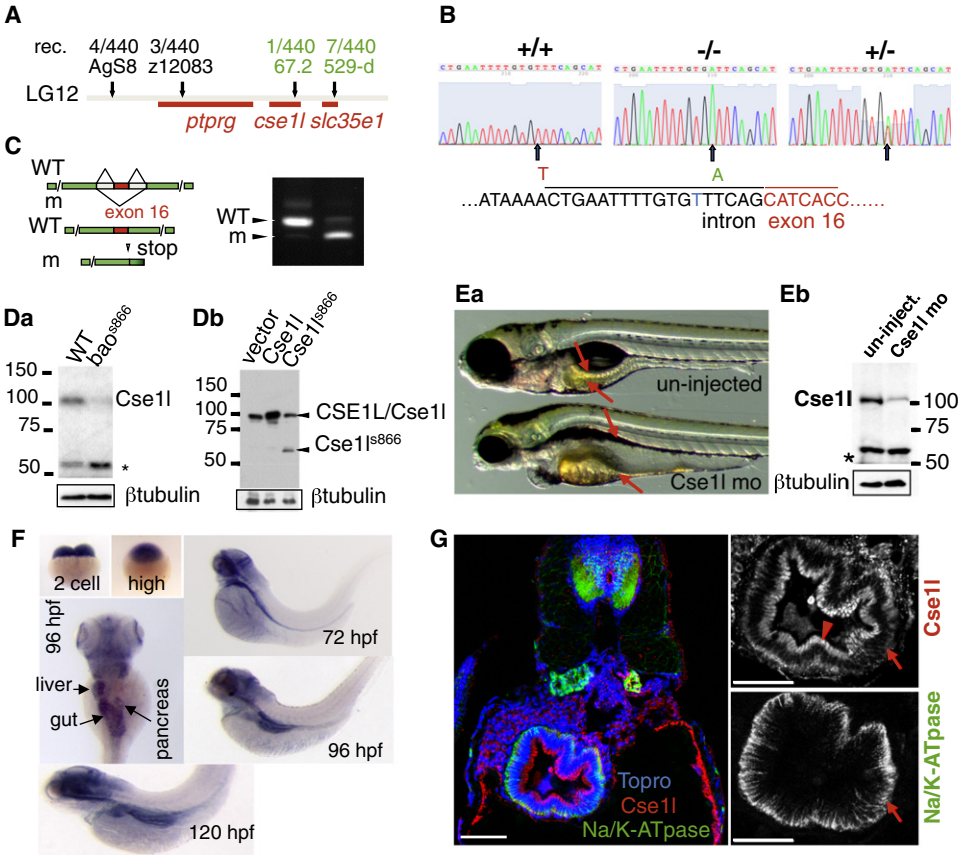


Figure 3. Isolation of the *bao* Gene

(A) Positional cloning of *bao*. The number of recombinants (rec.) for each marker is shown.
(B) Sequencing of genomic DNA from +/+, −/−, and +/− larvae revealed a T-to-A mutation (arrow) upstream of the exon 16 splice acceptor site.
(C) Reverse transcriptase PCR on pools of RNA made from WT and *bao*$^{s866}$ mutants demonstrates defective splicing of exon 16 in *bao*$^{s866}$ mutants leading to a premature stop codon in exon 17.
(Da) Cse1l is depleted in *bao*$^{s866}$ mutants. The asterisk marks the position of a cross-reacting protein band.
(Db) The *bao*$^{s866}$ mutation produces a truncated protein that can be detected in immunoblots of transfected HEK293 cells.
(Ea) Knockdown of Cse1l using an antisense morpholino targeting the translation start site phenocopies the *bao*$^{s866}$ mutation (22% penetrance at 5 days postfertilization [dpf], n = 220).
(Eb) Immunoblot of 5 dpf uninjected and Cse1l morphants demonstrating knockdown of this protein.
(F) In situ hybridization analysis using an antisense probe directed against the 3′ end and untranslated region of the *cse1l* mRNA.
(G) Immunofluorescence on WT sections showing Cse1l in the subapical (arrowhead) and basolateral (arrow) regions of intestinal cells at 120 hpf. Scale bars represent 50 μm.

agreement with the size prediction inferred from cDNA sequencing (Figure 3Db).

Next, we knocked down the expression of Cse1l and Ptprg using antisense morpholinos. Knockdown of Cse1l (Figure 3Ea), but not Ptprg (data not shown), phenocopied *bao*$^{s866}$. Immunoblot analysis confirmed that the phenotype of the Cse1l morphants showed a good correlation with the level of Cse1l depletion (Figure 3Eb). To determine the pattern of *cse1l* expression, we performed an in situ hybridization (ISH) analysis during WT development. The *cse1l* transcript was present at the two-cell stage (Figure 3F), indicating that it is maternally provided. Expression was broad early on but became restricted to the endoderm and parts of the brain by 48 hpf. At 96 hpf, *cse1l* was strongly expressed in the gut, liver, exocrine pancreas, and parts of the brain and retina (Figure 3F). Expression was strongest in the gut after 96 hpf, coinciding with the onset of the gut expansion phenotype. Thus, the expression pattern of *cse1l* shows a good correlation with the *bao*$^{s866}$ phenotype, affecting mostly gut, liver, and pancreas. To determine the subcellular localization of the Cse1l protein, we stained sections of 120 hpf WT larvae. At 120 hpf, Cse1l was found enriched in the gut and liver where we also found expression by ISH. The protein localized to the subapical and apical region of gut enterocytes and was also found associated with lateral and basal membranes (Figure 3G). Altogether, our data indicate that *bao* corresponds to *cse1l*.

Cse1l was originally isolated in a screen looking for regulators of chromosome segregation (hence the name) in yeast [17]. This highly conserved (86% identity and 93% similarity between zebrafish and humans) and essential gene [18] has been implicated in apoptosis [19], nuclear-cytoplasmic transport [20], cell-cell adhesion [21], and chromatin regulation [22]. Therefore, it seems likely that the cell delamination/apoptosis phenotype in *bao*$^{s866}$ mutants is linked to the nuclear and lateral membrane functions of Cse1l. However, the role of Cse1l in regulating CFTR-dependent fluid secretion is clearly separable from other functions (Figure 2Ab). Moreover,

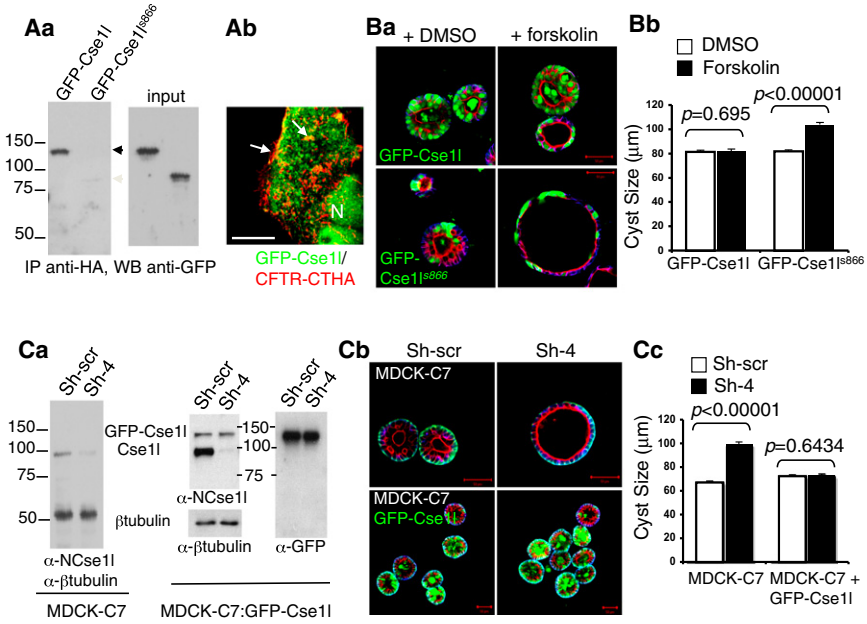


Figure 4. Cse1l Negatively Regulates Fluid Secretion in Mammalian MDCK-C7 Cells

(Aa) Zebrafish GFP-Cse1l, but not GFP-Cse1l$^{s866}$, coimmunoprecipitates with human CFTR-CTHA.

(Ab) Partial colocalization (arrows) of GFP-Cse1l and CFTR-CTHA in transfected HEK293 cells. N indicates nucleus. Scale bar represents 10 μm.

(B) Overexpression of zebrafish GFP-Cse1l abrogates the stimulatory effect of forskolin on CFTR-dependent fluid secretion in 3D cultures of mammalian MDCK-C7 cells.

(Ba) MDCK-C7 cells were grown on Matrigel for 4 days, and forskolin (1 μM) was then added for 16 hr before the cysts were fixed and imaged. Green is GFP, red is F-actin, and blue is β-catenin. Scale bars represent 50 μm.

(Bb) Quantification of data from (Ba) (n = 161 for GFP-Cse1l$^{s866}$; n = 131 for GFP-Cse1l). Error bars indicate standard error of the mean.

(C) Depletion of Cse1l leads to increased fluid secretion in 3D cultures of MDCK-C7 cells.

(Ca) Immunoblot showing knockdown of dog Cse1l in cells expressing a shRNA targeting Cse1l (Sh-4) but not in control cells expressing a nonsilencing shRNA (Sh-scr).

(Cb) Knockdown of dog Cse1l leads to lumen expansion in control but not in GFP-Cse1l-expressing MDCK-C7 cells in 3D cultures (5 days in Matrigel) following forskolin treatment. Red is F-actin, green is β-catenin in upper panels and GFP in lower panels, and blue is ToPro. Scale bars represent 50 μm.

(Cc) Quantification of data from (Cb) (n = 200 for control; n = 149 for GFP-Cse1l). Error bars indicate standard error of the mean.

zebrafish mutations in the nucleoporin gene *elys* trigger apoptosis in the gut but not fluid accumulation [23, 24].

Our data suggest a functional interaction between Cse1l and CFTR. To test whether these two proteins also interact physically, we performed coimmunoprecipitation experiments in HEK293 cells expressing human HA-tagged CFTR (CFTR-HA) [25] and GFP-Cse1l or GFP-Cse1l$^{s866}$. Notably, CFTR-HA coimmunoprecipitated with GFP-Cse1l but showed a much weaker interaction with GFP-Cse1l$^{s866}$ (Figure 4Aa). At the immunofluorescence level, a fraction of GFP-Cse1l colocalized with CFTR-HA (Figure 4Ab). We also coimmunoprecipitated endogenous CFTR and Cse1l from human intestinal Caco-2 cells (data not shown). Interestingly, a recent mass spectrometric analysis of CFTR-associated proteins identified CSE1L among several other potential CFTR partners in various human cell lines [26].

To investigate whether Cse1l regulates fluid secretion in mammalian cells, we employed a clone of Madin-Darby canine kidney (MDCK) cells that expresses endogenous CFTR (MDCK-C7) [27] and performed 3D cultures. When grown in Matrigel, these cells form hollow cysts that exhibit forskolin-stimulated, CFTR-dependent fluid transport and lumen expansion [9, 28]. Forskolin addition increases intracellular cAMP levels and stimulates protein kinase A, which in turn activates the CFTR channel through phosphorylation [29]. To test the effect of Cse1l overexpression and knockdown, we generated stable MDCK-C7 lines overexpressing GFP-tagged WT and mutant zebrafish Cse1l (GFP-Cse1l and GFP-Cse1l$^{s866}$, respectively) and examined the response to forskolin in 3D cultures. Cse1l is highly conserved between zebrafish and mammals, and the fish protein can functionally substitute for the mammalian protein (see below). Interestingly, although addition of forskolin (1 μM for 16 hr) led to a robust (25% increase in diameter; close to 200% increase in volume) and significant ($p < 0.00001$, n = 161) enlargement of control (vector only) or GFP-Cse1l$^{s866}$-expressing cysts, it did not affect the size of GFP-Cse1l-expressing cysts ($p = 0.695$, n = 131) (Figure 4). It is important to note that whereas cysts from cells transfected with vector only or GFP-Cse1l$^{s866}$ possessed mostly very thin (stretched) cells surrounding a single large lumen (100 μm on average), GFP-Cse1l-expressing cysts were mostly multilayered and contained multiple small lumens (1–10 μm). Thus, the difference in luminal volume was in fact much greater than the 200% increase derived from measurements of cyst diameter. Next, we knocked down (>80%) endogenous Cse1l expression via lentivirus-mediated expression of short hairpin interfering RNAs (shRNAs) (Figure 4Ca). The DNA sequence differences between zebrafish and dog Cse1l make the zebrafish construct insensitive to the shRNAs (Figure 4Ca). Upon Cse1l knockdown, we observed a robust (48% increase in diameter; more than 300% increase in total cyst volume) and significant ($p < 0.00001$, n = 200) expansion of the lumen that could be blocked by GFP-Cse1l expression ($p = 0.643$, n = 149). Finally, we assayed CFTR activity in HEK293 cells expressing CFTR by using a halide-sensitive YFP variant (YFP-H148Q) [30] and found that Cse1l overexpression strongly inhibited CFTR activity (Figure S4). Together, these experiments suggest that Cse1l is a negative regulator of CFTR activity in mammalian cells.

Altogether, our results are consistent with a scenario in which binding of Cse1l to CFTR results in the inhibition of the channel. Alternatively, Cse1l may be required for the function of a CFTR inhibitor. Although we cannot exclude an effect on the activity of other channels or channel cross-regulation, the physical interaction of Cse1l with CFTR suggests that Cse1l regulates CFTR activity directly.

Studies of CFTR function have relied mostly on cell culture and genetic association studies of populations of cystic fibrosis patients. Although these studies have provided valuable insights, an in vivo correlate has not yet been established. This work establishes zebrafish as a forward genetics

model system to study CFTR biology and demonstrates that these studies are translatable to mammalian models.

### Supplemental Information

Supplemental Information includes Supplemental Experimental Procedures and four figures and can be found with this article online at doi:10.1016/j.cub.2010.09.012.

### Acknowledgments

We thank B. Hogan, K. Poss, C. Penland, and Ç. Eroglu for critically reading the manuscript and A. Verkman for discussions and reagents. We are grateful to G. Lukacs, M. Gentzch, P. Haggie, and J. Riordan for reagents and constructs. M.B. was supported by a European Molecular Biology Organization long-term postdoctoral fellowship, and J.H. was supported by a Human Frontier Science Program postdoctoral fellowship. This work was funded in part by grant 0810 from the Cystic Fibrosis Foundation (CFF) and National Institutes of Health (NIH) Innovator Award 1DP2OD006486 to M.B., by the NIH (grants DK083330, DK074398, and P01AI53194 to K.M.; grant P30 DK065988 to S.G.; and grants DK60322 and DK075032 to D.Y.R.S.), and by the CFF and the Packard Foundation (D.Y.R.S.).

Received: May 26, 2010
Revised: August 5, 2010
Accepted: September 2, 2010
Published online: October 7, 2010

### References

1. Riordan, J.R. (2008). CFTR function and prospects for therapy. Annu. Rev. Biochem. *77*, 701–726.
2. Brown, P.D., Davies, S.L., Speake, T., and Millar, I.D. (2004). Molecular mechanisms of cerebrospinal fluid production. Neuroscience *129*, 957–970.
3. Riordan, J.R., Rommens, J.M., Kerem, B., Alon, N., Rozmahel, R., Grzelczak, Z., Zielenski, J., Lok, S., Plavsic, N., Chou, J.L., et al. (1989). Identification of the cystic fibrosis gene: Cloning and characterization of complementary DNA. Science *245*, 1066–1073.
4. Anderson, M.P., Gregory, R.J., Thompson, S., Souza, D.W., Paul, S., Mulligan, R.C., Smith, A.E., and Welsh, M.J. (1991). Demonstration that CFTR is a chloride channel by alteration of its anion selectivity. Science *253*, 202–205.
5. Gabriel, S.E., Brigman, K.N., Koller, B.H., Boucher, R.C., and Stutts, M.J. (1994). Cystic fibrosis heterozygote resistance to cholera toxin in the cystic fibrosis mouse model. Science *266*, 107–109.
6. Verkman, A.S., Lukacs, G.L., and Galietta, L.J. (2006). CFTR chloride channel drug discovery—inhibitors as antidiarrheals and activators for therapy of cystic fibrosis. Curr. Pharm. Des. *12*, 2235–2247.
7. McCole, D.F., and Barrett, K.E. (2003). Epithelial transport and gut barrier function in colitis. Curr. Opin. Gastroenterol. *19*, 578–582.
8. Sullivan, L.P., Wallace, D.P., and Grantham, J.J. (1998). Chloride and fluid secretion in polycystic kidney disease. J. Am. Soc. Nephrol. *9*, 903–916.
9. Li, H., Findlay, I.A., and Sheppard, D.N. (2004). The relationship between cell proliferation, Cl- secretion, and renal cyst growth: A study using CFTR inhibitors. Kidney Int. *66*, 1926–1938.
10. Yang, B., Sonawane, N.D., Zhao, D., Somlo, S., and Verkman, A.S. (2008). Small-molecule CFTR inhibitors slow cyst growth in polycystic kidney disease. J. Am. Soc. Nephrol. *19*, 1300–1310.
11. Ober, E.A., Verkade, H., Field, H.A., and Stainier, D.Y. (2006). Mesodermal Wnt2b signalling positively regulates liver specification. Nature *442*, 688–691.
12. Crosnier, C., Vargesson, N., Gschmeissner, S., Ariza-McNaughton, L., Morrison, A., and Lewis, J. (2005). Delta-Notch signalling controls commitment to a secretory fate in the zebrafish intestine. Development *132*, 1093–1104.
13. Pauls, S., Geldmacher-Voss, B., and Campos-Ortega, J.A. (2001). A zebrafish histone variant H2A.F/Z and a transgenic H2A.F/Z:GFP fusion protein for in vivo studies of embryonic development. Dev. Genes Evol. *211*, 603–610.
14. Huisken, J., Swoger, J., Del Bene, F., Wittbrodt, J., and Stelzer, E.H. (2004). Optical sectioning deep inside live embryos by selective plane illumination microscopy. Science *305*, 1007–1009.
15. Ma, T., Vetrivel, L., Yang, H., Pedemonte, N., Zegarra-Moran, O., Galietta, L.J., and Verkman, A.S. (2002). High-affinity activators of cystic fibrosis transmembrane conductance regulator (CFTR) chloride conductance identified by high-throughput screening. J. Biol. Chem. *277*, 37235–37241.
16. Gentzsch, M., Chang, X.B., Cui, L., Wu, Y., Ozols, V.V., Choudhury, A., Pagano, R.E., and Riordan, J.R. (2004). Endocytic trafficking routes of wild type and DeltaF508 cystic fibrosis transmembrane conductance regulator. Mol. Biol. Cell *15*, 2684–2696.
17. Xiao, Z., McGrew, J.T., Schroeder, A.J., and Fitzgerald-Hayes, M. (1993). CSE1 and CSE2, two new genes required for accurate mitotic chromosome segregation in Saccharomyces cerevisiae. Mol. Cell. Biol. *13*, 4691–4702.
18. Bera, T.K., Bera, J., Brinkmann, U., Tessarollo, L., and Pastan, I. (2001). Cse1l is essential for early embryonic growth and development. Mol. Cell. Biol. *21*, 7020–7024.
19. Behrens, P., Brinkmann, U., and Wellmann, A. (2003). CSE1L/CAS: Its role in proliferation and apoptosis. Apoptosis *8*, 39–44.
20. Kutay, U., Bischoff, F.R., Kostka, S., Kraft, R., and Görlich, D. (1997). Export of importin alpha from the nucleus is mediated by a specific nuclear transport factor. Cell *90*, 1061–1071.
21. Jiang, M.C., Liao, C.F., and Tai, C.C. (2002). CAS/CSE 1 stimulates E-cadhrin-dependent cell polarity in HT-29 human colon epithelial cells. Biochem. Biophys. Res. Commun. *294*, 900–905.
22. Tanaka, T., Ohkubo, S., Tatsuno, I., and Prives, C. (2007). hCAS/CSE1L associates with chromatin and regulates expression of select p53 target genes. Cell *130*, 638–650.
23. de Jong-Curtain, T.A., Parslow, A.C., Trotter, A.J., Hall, N.E., Verkade, H., Tabone, T., Christie, E.L., Crowhurst, M.O., Layton, J.E., Shepherd, I.T., et al. (2009). Abnormal nuclear pore formation triggers apoptosis in the intestinal epithelium of elys-deficient zebrafish. Gastroenterology *136*, 902–911.
24. Davuluri, G., Gong, W., Yusuff, S., Lorent, K., Muthumani, M., Dolan, A.C., and Pack, M. (2008). Mutation of the zebrafish nucleoporin elys sensitizes tissue progenitors to replication stress. PLoS Genet. *4*, e1000240.
25. Sharma, M., Pampinella, F., Nemes, C., Benharouga, M., So, J., Du, K., Bache, K.G., Papsin, B., Zerangue, N., Stenmark, H., and Lukacs, G.L. (2004). Misfolding diverts CFTR from recycling to degradation: Quality control at early endosomes. J. Cell Biol. *164*, 923–933.
26. Wang, X., Venable, J., LaPointe, P., Hutt, D.M., Koulov, A.V., Coppinger, J., Gurkan, C., Kellner, W., Matteson, J., Plutner, H., et al. (2006). Hsp90 cochaperone Aha1 downregulation rescues misfolding of CFTR in cystic fibrosis. Cell *127*, 803–815.
27. Lahr, T.F., Record, R.D., Hoover, D.K., Hughes, C.L., and Blazer-Yost, B.L. (2000). Characterization of the ion transport responses to ADH in the MDCK-C7 cell line. Pflugers Arch. *439*, 610–617.
28. Bagnat, M., Cheung, I.D., Mostov, K.E., and Stainier, D.Y. (2007). Genetic control of single lumen formation in the zebrafish gut. Nat. Cell Biol. *9*, 954–960.
29. Hallows, K.R., Kobinger, G.P., Wilson, J.M., Witters, L.A., and Foskett, J.K. (2003). Physiological modulation of CFTR activity by AMP-activated protein kinase in polarized T84 cells. Am. J. Physiol. Cell Physiol. *284*, C1297–C1308.
30. Galietta, L.J., Haggie, P.M., and Verkman, A.S. (2001). Green fluorescent protein-based halide indicators with improved chloride and iodide affinities. FEBS Lett. *499*, 220–224.